Applied Catalysis A, General 564 (2018) 113–122

Contents lists available at ScienceDirect

Applied Catalysis A, General

journal homepage: www.elsevier.com/locate/apcata

Deactivation of Sn-Beta during carbohydrate conversion

William N.P. van der Graaff[a], Christiaan H.L. Tempelman[a], Frank C. Hendriks[b], Javier Ruiz-Martinez[b,1], Sara Bals[c], Bert M. Weckhuysen[b,*], Evgeny A. Pidko[a,2,*], Emiel J.M. Hensen[a,*]

[a] Inorganic Materials Chemistry group, Schuit Institute of Catalysis, Eindhoven University of Technology, P.O. Box 513, 5600 MB, Eindhoven, The Netherlands
[b] Inorganic Chemistry and Catalysis Group, Debye Institute for Nanomaterials Science, Utrecht University, Universiteitsweg 99, 3584 CG, Utrecht, The Netherlands
[c] Electron Microscopy for Materials Science, University of Antwerp, Groenenborgerlaan 171, 2020, Antwerp, Belgium

ARTICLE INFO

Keywords:
Sn-Beta
Confocal fluorescence microscopy
Catalyst deactivation
Biomass conversion
Flow chemistry
Zeolite catalysis

ABSTRACT

The deactivation of Sn-Beta zeolite catalyst during retro-aldolization and isomerization of glucose is investigated. Confocal fluorescence microscopy reveals that retro-aldolization of glucose in CH_3OH at 160 °C is accompanied with the build-up of insoluble oligomeric deposits in the micropores, resulting in a rapid catalyst deactivation. These deposits accumulate predominantly in the outer regions of the zeolite crystals, which points to mass transport limitations. Glucose isomerization in water is not only accompanied by the formation of insoluble deposits in the micropores, but also by the structural degradation of the zeolite due to desilication and destannation. Enhanced and sustained catalytic performance can be achieved by using ethanol/water mixtures as the reaction solvent instead of water.

1. Introduction

Efficient conversion processes of renewable feedstocks into fuels and chemicals is pivotal to a more sustainable business model for the chemical industry. Biomass is an important source of renewable carbon with the potential to substitute fossil resources for the production of chemicals. In particular, the carbohydrate fraction of lignocellulosic biomass is considered a potential feedstock for future biorefinery processes, from which specific platform chemicals with a wide range of downstream applications can be produced (Fig. 1). This motivates researchers in industry and academia to search for new catalysts that can selectively promote the cascade reactions from cellulose via glucose towards platform molecules, such as 5-hydroxymethylfurfural (5-HMF) and lactic acid.

Zeolites functionalized with Lewis acid sites such as Sn-Beta are active catalysts for the isomerization of glucose to fructose, [1–6] which can be combined with acid-catalyzed dehydration of fructose to 5-HMF [7,8] and the retro-aldolization of C6 sugars and the conversion into lactic acid and derivatives [3,9–13]. Deactivation of the catalyst is a problem in all of these reactions. There are two main causes of deactivation, namely deposition of heavy by-products of the reactions and hydrothermal instability of zeolites. Retro-aldolization of C6 sugars is carried out at relatively high reaction temperature, resulting in the formation of undesired by-products. Several approaches have been followed to decrease this type of deactivation. For instance, alkali promoters modify the acidity towards a lower rate of deactivation [11]. Another approach is to synthesize more active catalysts that by operating at lower temperature produce less by-products [13]. Also, glucose conversion by zeolites results in deposition of by-products in the micropores [5]. A major problem is that reaction intermediates oligomerize via aldol-condensation reactions. The resulting oligomers/polymers are ill-defined compounds, usually called humins, which can block the catalyst surface [8,14]. As catalyst deactivation due to heavy product deposition is a general problem in zeolite catalysis [15–18], locating these species by spectroscopic methods has been pursued [19].

Concerning stability, catalyzing reactions with zeolites in hot liquid water can result in rapid deactivation [20,21]. The problem of stability of zeolite catalysts in sugar conversion has attracted a considerable attention in the recent years [4,22–27]. Hydrothermal conditions result in various chemical transformations due to hydrolysis of the zeolite framework, leading to a lower micropore volume and loss of active sites [28–32]. Pérez-Ramírez and co-workers investigated the stability of Sn-

* Corresponding authors.
E-mail addresses: b.m.weckhuysen@uu.nl (B.M. Weckhuysen), e.a.pidko@tudelft.nl (E.A. Pidko), e.j.m.hensen@tue.nl (E.J.M. Hensen).
[1] Current address: AkzoNobel - Supply Chain, Research & Development, Process Technology SRG, 7418 AJ Deventer, The Netherlands
[2] Current address: Inorganic Systems Engineering Group, Chemical Engineering Department, Delft University of Technology, Van der Maasweg 9, 2629 HZ Delft, the Netherlands

https://doi.org/10.1016/j.apcata.2018.07.023
Received 2 May 2018; Received in revised form 9 July 2018; Accepted 17 July 2018
Available online 21 July 2018

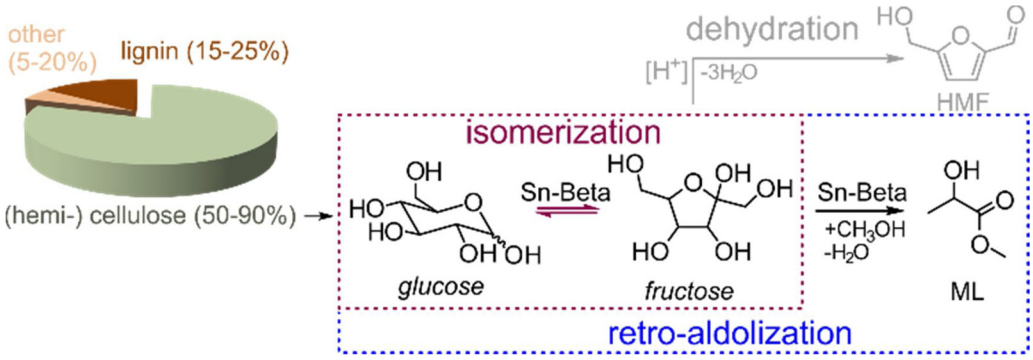

Fig. 1. Cellulose and hemicellulose constitute the major fraction of lignocellulosic biomass that can be converted to platform chemicals such as 5-hydroxymethylfurfural (HMF) and methyl lactate (ML). Glucose to fructose isomerization is the key step in both conversion paths. Lewis acid sites in Sn-Beta catalyse both the aldose-ketose isomerization to fructose and subsequent retro-aldolization reaction yielding ML. Fructose dehydration to HMF proceeds over a Brønsted acid catalyst.

containing Beta and MFI zeolite prepared by isomorphous substitution and post-synthetic Sn introduction [33,34]. Zeolites prepared by isomorphous substitution during zeolite synthesis were more stable than those prepared by post-synthetic introduction of Sn. Hammond and co-workers investigated the stability of post-synthetically modified Sn-Beta in a range of reactions related to biomass valorization [21]. Only when carrying out the catalytic reaction in non-aqueous media, a reasonable catalyst lifetime could be achieved. However, it was also reported by Hammond and co-workers that addition of minor amounts of water in a methanol/sugar feed led to increased catalyst activity and stability, while pure water was found to be detrimental for the catalytic performance [54]. Furthermore, the same group found that deactivation proceeds faster when the Sn-sites are dehydrated rather than hydrated [56]. In all, there are many factors contributing to deactivation of zeolites in sugar conversion reactions. Therefore, it is necessary to further elucidate deactivation mechanisms in zeolite-catalyzed sugar conversion.

In this study, we present the results of a systematic investigation of the deactivation of Sn-Beta zeolite during sugar conversion. We first investigated the structural and textural changes in Sn-Beta zeolite during retro-aldolization of glucose at 160 °C. Confocal fluorescence microscopy on large crystals of spent Sn-Beta and Al-Beta zeolites were used to visualize the intra-zeolite deposits [35,36]. Despite the limited utility of the Brønsted acidic Al-Beta catalysts for the selective sugar conversions, these materials provide a better resolved benchmark systems for probing the transport of bulky sugar molecules and subsequent growth of insoluble deposits inside the zeolite micropores. Next, we investigated the catalytic stability and the origin of deactivation of Sn-Beta during sugar (glucose and 1,3-dihydroxyacetone) isomerization under milder conditions (70–100 °C). Finally, we demonstrated that the use of a mixture of ethanol and water as a solvent allows more stable operation during glucose isomerization by Sn-Beta.

2. Experimental

2.1. Chemicals

Tetraethyl orthosilicate (TEOS, > 99%, Merck), tetraethylammonium hydroxide (TEAOH, 35% solution in water, Sigma Aldrich), $SnCl_4.5H_2O$ (98%, Sigma-Aldrich), anhydrous $SnCl_4$ (99%, Aldrich), HF (40% in water, Merck), $Al(O^iPr)_3$ (> 98%, Aldrich), Ludox SM-30 (Sigma Aldrich), methanol (AR grade, BioSolve), D-glucose (> 99.5%, Sigma), 1,3-dihydroxyacetone (DHA, dimeric form, > 97%, Sigma Aldrich), HNO_3 (65% in water, Merck) and lactic acid (90%, BDH Prolabo) were used as received without further purification.

2.2. Catalyst synthesis

2.2.1. Sn-Beta-HF-large

Large crystals of Sn-Beta zeolite were synthesized according to an established literature procedure [5]. Tetraethylorthosilicate (TEOS) (14.03 g, 1 eq.), TEAOH (15.42 g 35 wt% solution, 0.54 eq.) and $SnCl_4{\cdot}5H_2O$ (0.24 g, 0.01 eq.) were mixed in a Teflon beaker until a clear, homogeneous gel was obtained. After evaporation of ethanol and part of the water, HF (40% in water, 1.5 mL, 0.50 eq.) was added to yield a dry gel with a final composition of 1 SiO_2 : 0.54 TEAOH : 0.50 H F : 0.01 $SnCl_4$: 7.5 H_2O. The mixture was transferred to a Teflon-lined steel autoclave and heated in static mode for 40 days at 140 °C. Subsequently, the material was washed and dried in air. Calcination at 550 °C for 10 h (1 °C/min) in static air yielded the final material.

2.2.2. Al-Beta-HF-large

Tetraethylorthosilicate (TEOS) (14.03 g, 1 eq.), TEAOH (15.42 g 35 wt% solution, 0.54 eq.) and $Al(O^iPr)_3$ (0.27 g, 0.02 eq) were mixed in a Teflon beaker until a clear, homogeneous gel was obtained. After evaporation of ethanol and part of the water, HF (40% in water, 1.5 mL, 0.50 eq.) was added to yield a dry gel with a final composition of 1 SiO_2:0.54 TEAOH : 0.50 H F : 0.02 Al: 7.5 H_2O. The mixture was transferred to a Teflon-lined steel autoclave and heated in static mode for 40 days at 140 °C. Subsequently, the material was washed and dried in air. Calcination at 550 °C for 10 h (1 °C/min) in static air yielded the final material.

2.2.3. Sn-Beta-HF

Small-crystalline Sn-Beta-HF was synthesized using the seed-promoted procedure as described elsewhere [37]. Tetraethylorthosilicate (TEOS) (14.03 g, 1 eq.), TEAOH (15.42 g 35 wt% solution, 0.54 eq.) and $SnCl_4.5H_2O$ (0.24 g, 0.01 eq.) were mixed in a Teflon beaker until a clear, homogeneous gel was obtained. After evaporation of ethanol and part of the water, HF (40% in water, 1.5 mL, 0.50 eq.) was added to yield a dry gel with a final composition of 1 SiO_2 : 0.54 TEAOH : 0.50 H F : 0.01 $SnCl_4$: 7.5 H_2O. 40 mg of nanosized Beta-seeds was added and thoroughly homogenized. The mixture was transferred to a Teflon-lined steel autoclave and heated in a rotation oven (20 rpm) for 20 days at 140 °C. Subsequently, the material was washed and dried in air. Calcination at 550 °C for 10 h (1 °C min^{-1}) in static air yielded the final material.

2.2.4. Post-synthetic nano Sn-Beta (Sn-Beta-100)

Sn-Beta-100 was prepared as described elsewhere [38]. Nano-sized Al-Beta zeolite precursors with synthesis Si/Al ratio of 100 were prepared according to a modified procedure reported by Mintova et al. [39] To 37 *g* of Ludox SM-30, a solution of TEAOH in water (28.1 *g*) and $Al(OiPr)_3$ (0.38 *g*) were added and the mixture was stirred for 20 h, after which a clear solution was formed. The mixture was subsequently transferred to a Teflon-lined steel autoclave and placed in an oven at 100 °C for 18 days under static conditions. The resulting zeolite was collected by centrifugation, washed thoroughly with water and dried in air. The zeolite was calcined at 400 °C and 550 °C (both 1 °C min^{-1}, 10 h), successively. Dealumination was performed by refluxing in 65% HNO_3 (50 mL g^{-1}) at 110 °C overnight. Residual HNO_3 was removed by thorough washing with demineralized water until the pH of the

Table 1
Physicochemical properties of spent Sn-Beta-HF-large and Al-Beta-HF-large (retro-aldolization glucose in methanol at 160 °C) and yield of methyl lactate.[a].

Catalyst	t (h)	V_{micro} (cm^3/g)	V_{meso} (cm^3/g)	S_{BET} (m^2/g)	Y_{ML} (%)[b]	Weight loss (%)[c]
Al-Beta-HF-large	0	0.22	0.02	516	–	–
	16	0.07	0.02	199	< 1*	7.8
Sn-Beta-HF-large	0	0.19	0.04	530	–	–
	1	0.09	0.02	234	18	6.3
	2	0.13	0.05	359	19	6.7
	4	0.10	0.05	297	22	6.2
	8	0.08	0.03	225	21	6.4
	16	0.13	0.04	331	23	7.7

[a] Conditions: 80 mg catalyst, 112 mg glucose, 160 °C, in 5 ml MeOH solvent.
[b] ML = methyl lactate.
[c] Determined by TGA weight loss upon hearing from 150 °C to 750 °C at 5° min^{-1} ramp in O_2.

washings was neutral. Prior to modification with Sn, the dealuminated Beta zeolite was dried in vacuo at 170 °C for 3 h in a Schlenk flask. Sn was incorporated by adding an excess of about 3 silanol nest equivalents of anhydrous $SnCl_4$ at 100 °C under an Ar atmosphere and the mixture was stirred overnight. In order to remove unreacted $SnCl_4$ from the zeolite pores, the materials were thoroughly washed with methanol at least six times and dried in air. In order to remove residual chloride and to complete the condensation of the Sn centers into the framework, the material was recalcined at 550 °C (1 °C min^{-1}, 5 h). The final Sn-modified catalyst is denoted as Sn-Beta-100.

2.3. Characterization

X-ray diffraction patterns were recorded on a Bruker D2 diffractometer using Cu Kα radiation in the 2θ range 5–60° with a scanning speed of 0.01° s^{-1}. Elemental analyses were carried out using a Spectro Ciros CCD ICP optical emission spectrometer with axial plasma viewing. For analysis the materials an equivolumetric mixture of HF (40 wt% in water), HNO_3 (65 wt% in water) and water was used as matrix. Thermogravimetric analyses to determine the water content of the zeolites were done on a Mettler TGA/DSC-1 apparatus using 70 µL alumina crucibles. Helium was used at a gas flow rate of 40 mL min^{-1} and oxygen at a rate of 20 mL min^{-1}. Samples were heated from 25 °C to 750 °C at a heating rate of 5 °C min^{-1}. Argon physisorption measurements were performed at −186 °C on a Micromeritics ASAP2020 apparatus in static measurement mode. In a typical experiment, a zeolite sample (typically 100 mg) was outgassed at 350 °C for 8 h prior to the measurement. The Brunauer-Emmett-Teller (BET) equation was used to calculate the specific surface area from the adsorption data in the p/p0 range 0.05-0.35. The mesopore volume was calculated by applying the Barrett-Joyner-Halenda (BJH) method on the adsorption branch of the isotherm and the micropore volume was calculated by using the t-plot method. Scanning electron microscopy (SEM) was performed using a Philips environmental FEIXL-30 ESEM FEG in high-vacuum mode at low voltage. FT-IR measurements were performed on a Bruker Vertex V70v system. The spectra were acquired as an average of 64 scans at a resolution of 2 cm^{-1}. The samples were prepared by dilution in KBr. The spectra were recorded after 15 min in vacuum and are normalized by weight. UV–vis spectra of the catalyst were recorded using an Avantes Avalight DH-S-BAL with deuterium and halogen lamps as light source and an Avantes Avaspec 2048 L detector. The spent catalysts were referenced to the fresh materials, the fresh catalyst was referenced to a halon white background.

SEM-FIB measurements were carried out by etching the crystals with a Ga-ion beam (Focused Ion Beam, FEI Helios Nanolab 650). SEM images were recorded using a FEI Quanta FEG 250 at low pressure.

Confocal fluorescence microscopy measurements and mapping were performed on a Nikon Eclipse 90i upright microscope using a 100x/0.70 NA dry objective. The microscope is equipped with a Nikon-Eclipse A1R scan head. Confocal fluorescence images were recorded using excitation from two laser light sources: a Melles Griot Argon ion 488 nm laser providing 40 mW (detection in the range of 518–710 nm) and a Coherent Sapphire 561 nm solid state laser providing 50 mW (detection in the range of 591–750 nm). Emitted fluorescence was detected by a spectral detection unit equipped with a diffraction grating and a 32 photomultiplier tube array.

2.4. Catalytic activity tests

2.4.1. Retro-aldol reaction

The retro-aldolization of hexoses was performed by mixing 80 mg of zeolite, 112 mg of glucose and 4 g methanol in a stainless-steel autoclave containing a Teflon-lined magnetic stirring bar. The reactor was then heated to 160 °C. After the reaction, the autoclave was quenched rapidly in an ice bath. After filtration, the reaction mixture was analyzed by GC-FID using n-decane as external standard.

2.4.2. Glucose isomerization

Batch reaction experiments were carried out in 4 mL thick-walled glass vials that were loaded with 40 mg zeolite and 2.5 mL of a 125 mM aqueous glucose solution. The vessel was heated in an oil bath to the desired temperature and quenched in ice. The reaction mixture was analyzed by HPLC using a Prevail Carbohydrate column (Grace, 4.6 x 250 mm column, 5 µm particle size) coupled to a Shimadzu ELSD-II detector. CH_3CN:H_2O 65:35 was used as mobile phase (0.75 mL/min). ELSD settings were 50 °C and 3.5 bar N_2.

Continuous sugar isomerization experiments were carried out in a fixed-bed stainless-steel tubular reactor with an internal diameter of 7 mm heated by an oven. The Sn-Beta-catalysts were pelletized by applying a pressure of 156 MPa followed by grinding and sieving. The fraction of 250–500 µm was used for activity measurements. In a typical experiment, 125–250 mg was loaded in the reactor and flushed for 16 h with water at ambient conditions. Then the feed was replaced by a 125 mM glucose solution and the reactor was heated to the desired reaction temperature. All reactions were run for 50 h. The reactions were carried out at slightly elevated pressure by using a back-pressure regulator, whose pressure was set slightly above the autogenous pressure of water at the reaction temperature. Samples were regularly analyzed by HPLC (same settings as for the batch reaction mixtures). The spent catalysts were recovered and extensively washed with water or methanol and dried in air.

3. Results and discussion

3.1. Glucose retro-aldolization

The deactivation of Sn-Beta in the retro-aldolization reaction of glucose was investigated using Sn-Beta and Al-Beta as model samples. The samples were prepared by a fluoride-assisted method [5], resulting in large crystals amenable to spatially resolved fluorescence microscopy. Scanning electron microscopy (SEM) showed that the zeolite crystals of Sn-Beta-HF-large and Al-Beta-HF-large have dimensions of ca. 7 µm and 18 µm, respectively (Fig. S1). A typical capped bipyramidal crystal shape is observed for Al-Beta-HF-large, while Sn-Beta-HF-large is comprised of elongated crystallites with pronouncedly rounded edges in keeping with literature [40]. X-ray diffraction analysis confirms the high crystallinity of the Beta samples (Fig. S1c). Elemental analysis showed that the Si/Sn and the Si/Al ratios of the two samples were 108 and 41, respectively. SEM/EDX elemental mapping of cut crystals showed a homogeneous distribution of the heteroatoms across the zeolite crystals. Figure S2 shows representative SEM images and associated EDX elemental maps of Al-Beta-HF-large (Fig. S2a) and Sn-Beta-HF-large (Fig. S2b) samples after etching with Ga^+ ion beam.

Catalytic performance data of glucose conversion at 160 °C in

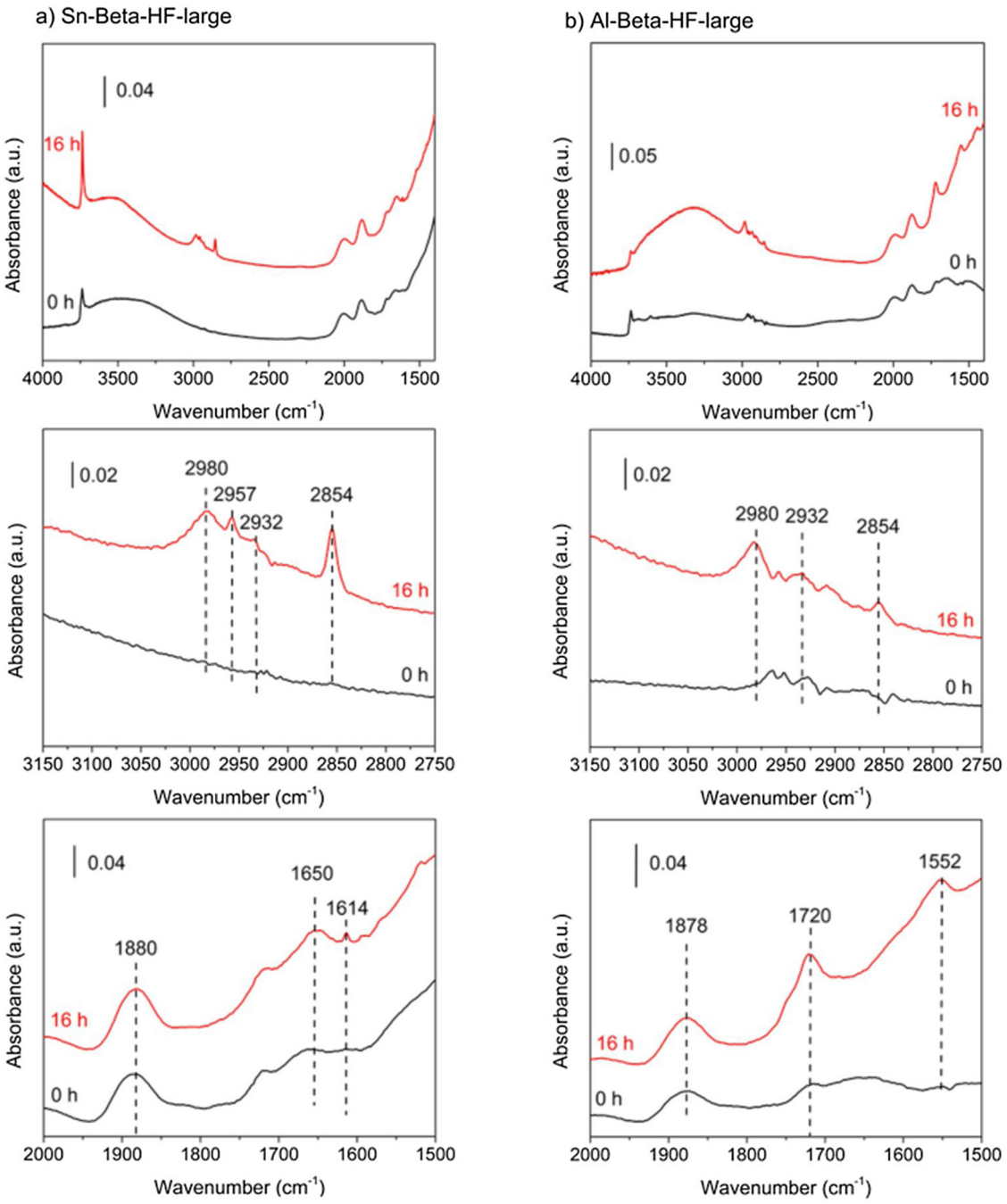

Fig. 2. IR spectra of a) Sn-Beta-HF-large and b) Al-Beta-HF-large before and after use in glucose conversion in methanol at 160 °C. Spectra were recorded at room temperature after evacuation for 15 min and normalized by weight of the sample. The red lines correspond to the spent sample after 6 h of reaction, the black lines to the calcined, fresh zeolites.

methanol and changes in the textural properties are provided in Table 1. The Lewis acidic Sn-Beta zeolite showed a good activity in retro-aldolization of glucose, providing an 18% methyl lactate yield after 1 h reaction which did not change appreciably when the reaction was prolonged. The H-Beta did not catalyse the retro-aldolization reaction, but instead methyl levulinate was obtained in 38% yield after 1 h. The reactions in methanol at 160 °C had a profound impact on the physico-chemical properties of Sn-Beta-HF-large and Al-Beta-HF-large samples. Both zeolites suffer from a substantial decrease of the surface area. TGA of the spent samples indicates that the deposition of insoluble deposits in the micropores is one of the causes for this decline in micropore surface area. The more detailed time-on-stream analysis for Sn-Beta shows that most of the ML-forming reaction took place in the first hour of the reaction. This suggests that already at the early stages of the reaction, the pore openings of the zeolite crystallites become blocked. The rapid deactivation can be correlated to the large size of the zeolite crystals with a high bulk-to-surface ratio. This can explain the lower than expected ML yield compared to conventional Sn-Beta catalysts (ca. 38% ML yield under identical conditions) [11,12,41].

We used IR spectroscopy to gain a better insight into the structural changes of the zeolite and the nature of the species deposited inside the zeolite pores during glucose reaction. The IR spectrum of spent Sn-Beta-HF (Fig. 2a) shows a pronounced increase of the 3740 cm^{-1} band due to terminal silanol groups, whereas the broad band in the 3200-3600 cm^{-1} region due to hydrogen-bonded silanols changes only slightly. An opposite effect is observed for spent Al-Beta-HF-large: the

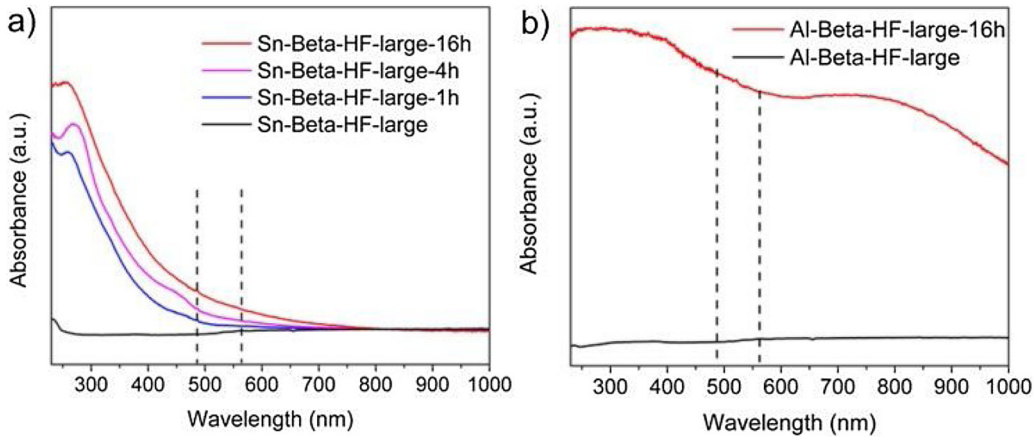

Fig. 3. UV–vis spectra of spent a) Sn-Beta-HF-large and b) Al-Beta-HF-large after use in the conversion of glucose in methanol at 160 °C. The dashed lines indicate the excitation wavelengths of 488 nm and 561 nm used for confocal fluorescence microscopy.

hydrogen-bonded hydroxyl groups undergo more pronounced changes than the silanol groups. Sugar conversion in Sn-Beta-HF-large gives rise to a set of new bands in the ν_{CH} region with maxima at 2854 cm^{-1}, 2932 cm^{-1}, 2957 cm^{-1} and 2980 cm^{-1} attributed to CH_2- and CH_3-groups of the deposits. The presence of CH_3 groups can by related to condensation of the products with methanol or formation of lactates [42–44]. The band at 2957 cm^{-1}, which is absent in the IR spectrum of spent Al-Beta-HF-large, is most likely due to adsorbed lactate species. The reaction over Al-Beta-HF-large gives rise to intense bands with maxima at 1552 cm^{-1} and 1720 cm^{-1} attributable to C═C and C═O moieties, respectively. These bands point to the formation of oligomerized aromatic, possibly furanic, species [45] and methyl levulinate [46,47] upon Brønsted acid-catalyzed conversion of glucose at elevated temperature. The changes in the low-frequency part of the spectrum of the spent Sn-Beta-HF-large sample are relatively minor. On the other hand, the intensity of the bands at 1614 cm^{-1} and 1650 cm^{-1} characteristic for C═C moieties formed by the dehydration side-reactions is increased [45]. There are no large amounts of free methanol in the pores as follows from the absence of the OH-deformation band around 1680 cm^{-1} [48]. The characteristic band at 1630 cm^{-1} due to the γ_{H2O} vibrational mode of adsorbed water was also not observed.

UV-Vis spectroscopy provides further evidence for the presence of aromatic oligomers in spent Al-Beta-HF-large by the broad and strong absorption band at 750 nm (Fig. 3) [45,49]. The spent Sn-Beta-HF-large catalyst contains much less of these polyaromatic species. The increasing absorption in the UV-region (ca. 300 nm) for this catalyst should rather be attributed to the formation of relatively low-molecular weight furanic oligomers inside the zeolite pores [45].

We further investigated the location of these carbon deposits in spent Sn-Beta-HF-large by confocal fluorescence microscopy (Fig. 4). Confocal fluorescence maps were taken after recovery at different reaction times of glucose in methanol at 160 °C. Laser excitation with wavelengths of 488 nm and 561 nm (indicated with dashed lines in the UV–vis spectra in Fig. 4) were used to localize the deposits. The possible formation of extraframework Sn species in the spent catalysts is not expected to influence the fluorescence intensities because such species typically have absorption wavelengths below 450 nm [38,55]. The confocal maps presented in Fig. 4a-c indicate the predominant build-up of the fluorescent species at the edges of the zeolite crystal. A similar pattern has also been observed for zeolite deactivation during etherification of olefins with glycerol by Parvulescu et al. [19] From TGA, no substantial increase in the amount of the deposits was observed after 1 h reaction. In the fluorescence maps shown in Fig. 4a these species appear to be uniformly distributed. After 4 h reaction, an egg-shell distribution evolves. We assume that the increase of the fluorescence signal at the edge at longer reaction time is due to further oligomerization of sugar deposits already present after 1 h of reaction (Fig. 4a). This could be linked to the higher concentration of Sn-sites towards the edge of the catalyst particles, where coke forms much faster than in the core of the particle. After 16 h reaction, a more uniform distribution is observed again due to further growth of the depositions throughout the particle. In a comparable experiment with Al-Beta-HF-large catalysts, a much more homogeneous distribution of the fluorescent signal due to insoluble deposits was observed. We speculate that the reason for such a different picture observed for the two materials is a lower sugar oligomerization on Brønsted acid sites than over Lewis acid sites allowing for a deeper penetration of glucose molecules inside the zeolite particle.

3.2. Glucose isomerization

Next, we investigated the stability of Sn-Beta during glucose to fructose isomerization reaction in water. This reaction can be carried out at lower temperature. The use of water is challenging for the stability of zeolites and also leads to by-product formation. The catalytic performance of Sn-Beta-HF in glucose isomerization was first investigated in a batch reactor. Fig. 5 shows the yields of glucose, fructose and mannose and the carbon balance as a function of the reaction time for Sn-Beta-HF. We confirmed that under otherwise identical conditions, the use of Al-Beta-HF did not result in any glucose conversion after 6 h. The steady decrease of the carbon balance goes together with a darkening of the zeolite particles and a decrease of the pH of the reaction mixture to 3–4. The formation of deposits was investigated by IR spectroscopy (Fig. 6), UV–vis spectroscopy (Fig. 7) and confocal fluorescence microscopy (Fig. 8).

The spent samples used in glucose conversion in water at 100 °C were heated to 200 °C for 1 h in order to oligomerize the remaining carbohydrates and other products. Such a procedure was employed to better visualize the presence of reactant and product molecules by confocal fluorescence microscopy. We first discuss IR spectra of these spent samples (Fig. 6). Similar to the spent zeolites used in retro-aldolization, we observed a strong increase in the amount of silanol groups (3740 cm^{-1}), which is due to formation of lattice defects. The silanol signal decreases again following the thermal treatment at 200 °C. This suggests that the silanol defects can react with OH-groups of the organic deposits. The strong absorption in the 3200-3600 cm^{-1} region is due to physisorbed water. Upon heating to 200 °C, signature bands of CH_3 and CH_2 groups appear in the 2800-3000 cm^{-1} range. Specific to spent Sn-Beta-HF-large, bands at 1780 cm^{-1}, 1662-1677 cm^{-1} and 1521 cm^{-1} appear after glucose isomerization at 100 °C. The bands at 1677 cm^{-1} and 1521 cm^{-1} can be attributed to the C═O and C═C stretching vibrations in 5-HMF, respectively [50].

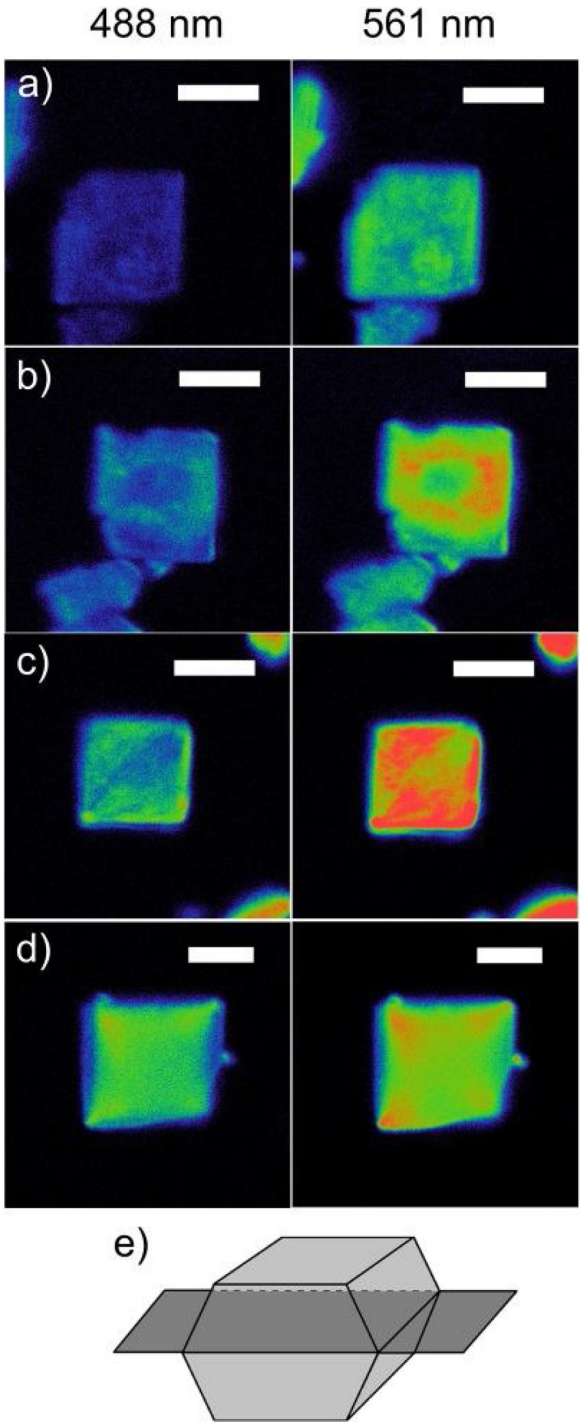

Fig. 4. Spatial distribution of carbonaceous deposits in single crystals of spent catalysts after reaction of glucose at 160 °C in methanol. Images were taken in the middle of the crystal. For the visualization of deposits, 488 nm and 561 nm lasers were used with a detection range of 518–710 nm and 591–750 nm, respectively. Confocal fluorescence microphotographs are presented in false colors (intensities are all boosted with the same factor for the individual lasers). Images of Sn-Beta-HF-large after a) 1 h, b) 4 h c) 16 h of reaction (scale bar 5 μm) and d) Al-Beta-HF-large after 16 h of reaction of glucose (scale bar 10 μm). The images on the left were recorded upon excitation at 488 nm, the lower images at 561 nm. All settings were kept the same across all images. e) A schematic representation of the cross section of the crystal in the middle plane.

This shows that the formation of furanic deposits already takes place under mild conditions. The signal at 1637 cm^{-1} for spent Al-Beta-HF-large is most likely due to water [51]. This signal is only present as a weak shoulder in spent Sn-Beta-HF-large and disappears in both samples after heating the sample at 200 °C.

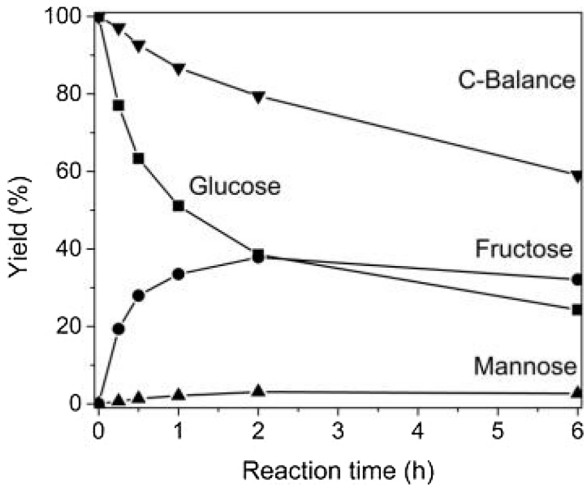

Fig. 5. Glucose isomerization over Sn-Beta-HF in a batch reactor (conditions: 100 °C, 40 mg Sn-Beta-HF, 2.5 mL water, 125 mM glucose).

The UV–vis spectra (Fig. 7) show the development of absorption bands at higher wavelengths following thermal treatment at 200 °C. This confirms oligomerization of molecular species present in the micropores. Absorption at high wavelength is much stronger for Sn-Beta-HF-large than for Al-Beta-HF-large. The absence of oligomeric species for the latter zeolite is due to the low conversion of glucose under the mild conditions of isomerization.

The formation of deposits in the zeolite micropores upon glucose isomerization in water at 100 °C was visualized by confocal fluorescence microscopy (Fig. 8). The fluorescence signals for spent Sn-Beta-HF-large are very weak (Fig. 8a). The observed species are most likely derived from reactions between sugars amongst themselves and with by-products such as 5-HMF [14]. This is in line with the observation of furanic species in the IR spectra (Fig. 6a). On contrary, Al-Beta-HF-large did not yield fluorescent species after 6 h reaction in glucose at 100 °C (Fig. 8c). This is in line with a glucose conversion less than 1% for this sample. Upon heating the spent Al-Beta-HF-large sample at 200 °C for 1 h, the fluorescence signal was observed throughout the crystal (Fig. 8d), which is in line with the UV–vis absorption spectra. The presence of fluorescent species confirms that sugars and other reaction intermediates are located in the micropores, which can be involved in further oligomerization reactions.

We can thus infer that the side-products are responsible for the decrease in the carbon balance and can give rise to the formation of deposits under the applied conditions (Fig. 5). These results emphasize the susceptibility of Sn-containing zeolites to deactivation via pore-blocking due to the build-up of carbonaceous deposits inside the micropores under the reaction conditions. Batch experiments are not suitable to assess catalyst stability. Therefore, we also determined the activity of Sn-Beta as a function of the time on stream in a flow reactor, focusing on the role of the sugar, the temperature and the solvent.

We first investigated glucose isomerization with Sn-Beta-HF at a temperature of 100 °C and a WSHV of 0.7 h^{-1}. Under these reaction conditions, fructose was the main reaction product and only very small amounts of mannose were observed. As follows from Fig. 9, the isomerization activity decreased strongly with reaction time. Deactivation was most pronounced during the first 6 h of the reaction. After 24 h on stream, about 70% of the initial activity was lost. Glucose conversion and fructose yield stabilized at ~20% and ~15%, respectively.

Calcination of the spent catalyst in flowing air at 550 °C could partially restore the initial activity. The revived catalyst also deactivated at a nearly similar rate (Fig. 9b). The textural properties collected in Table 2 show that the loss of micropore volume after the glucose

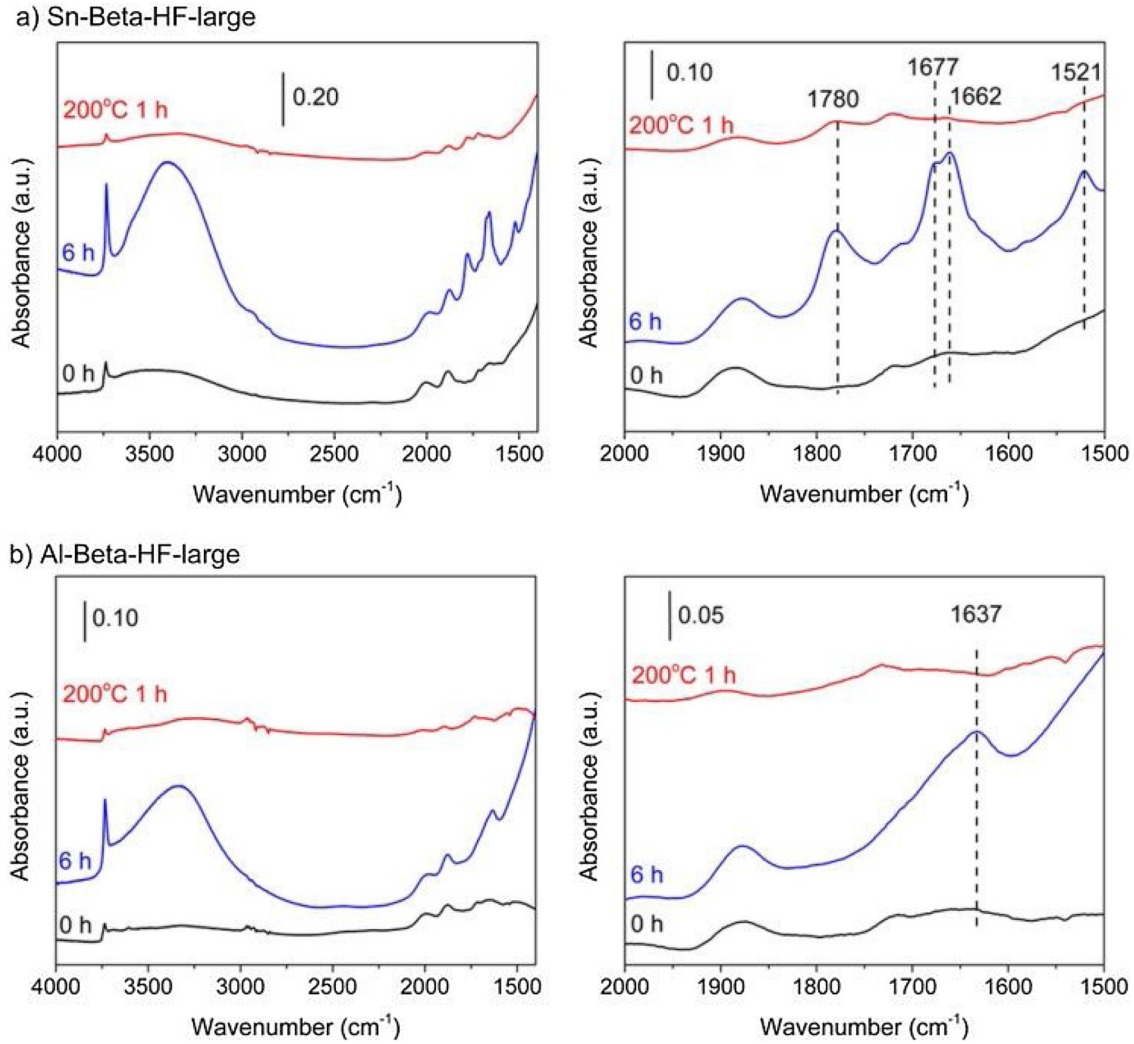

Fig. 6. IR spectra of a) Sn-Beta-HF-large and b) Al-Beta-HF-large before (black line) and after (blue line) reaction of glucose in water at 100 °C for 6 h and subsequent heating at 200 °C for 1 h (red line). The spectra were recorded after 15 min of evacuation and normalized by weight.

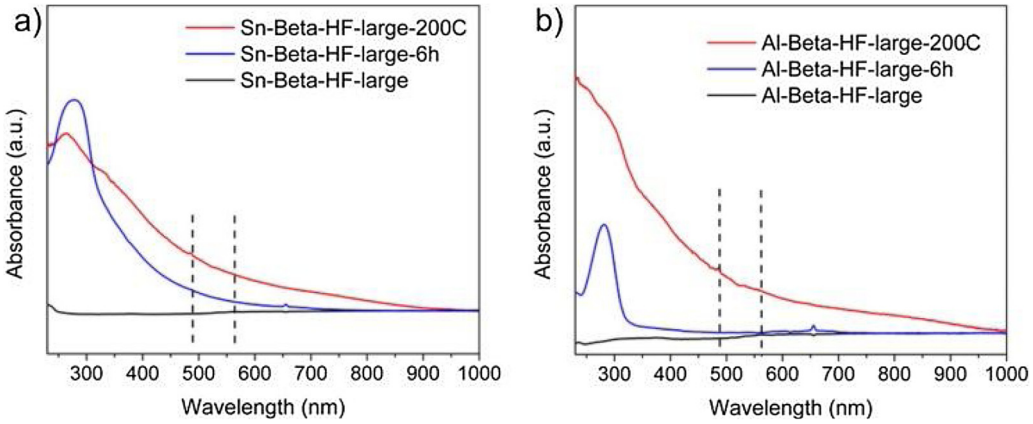

Fig. 7. UV–vis spectra of a) Sn-Beta-HF-large and b) Al-Beta-HF-large before (black line) and after 6 h isomerization (blue line) and subsequent heating at 200 °C for 1 h (red line). The dashed lines indicate the excitation wavelengths of 488 nm and 561 nm used for confocal fluorescence microscopy (Fig. 8).

conversion experiment was mainly due to the formation of deposits, as calcination led to a nearly identical micropore volume as for the fresh catalyst. On the other hand, the calcined spent catalyst contained a larger amount of mesopores than the fresh catalyst, which increased further upon reuse. This strongly suggests that the zeolite framework was damaged under the hydrothermal reaction conditions. Elemental analysis shows that the glucose conversion reaction did not lead to leaching of Sn (Table 2). We found that the deactivation mechanism of a post-synthetically modified Sn-Beta was different. The deactivation of this sample was much more pronounced and the textural properties of this catalyst was irreparably impeded (Table S1 and Fig. S4). It is likely that the high silanol density of this sample contributes to the poor

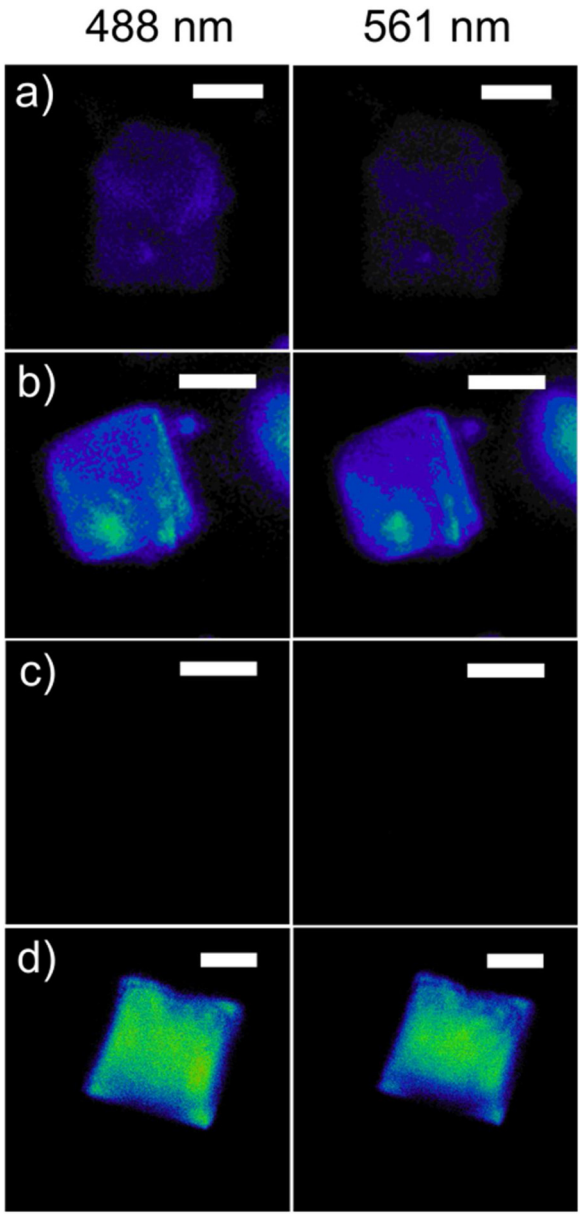

Fig. 8. Spatial distribution of deposits in single zeolite crystals of spent catalysts. Confocal fluorescence microphotographs are presented in false colors and the intensities are all boosted with the same factor for the individual lasers used. Confocal fluorescence microphotographs of Sn-Beta-HF-large after a) 6 h isomerization in water at 100 °C and b) heating the spent catalyst at 200 °C for 1 h (scale bar 5 µm); Al-Beta-HF-large after c) 6 h of isomerization in water and d) heating at 200 °C for 1 h (scale bar 10 µm). For recording the top images an excitation wavelength of 488 nm was used, for the lower images a 561 nm laser was used. Detection ranges were 518–710 nm and 591–750, respectively, for these two laser lines.

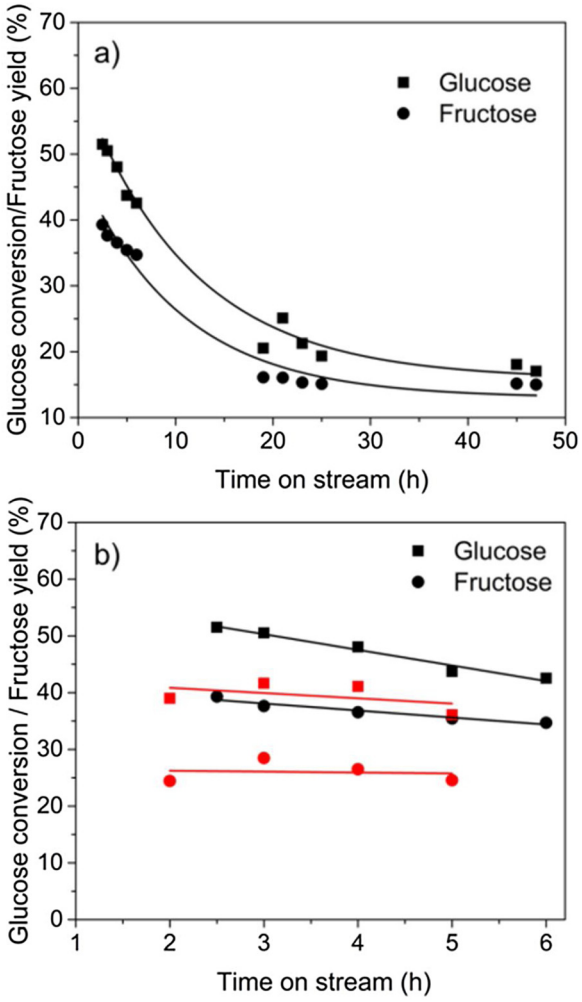

Fig. 9. Isomerization of glucose to fructose in flow with fresh (a) and fresh versus calcined spent (b) Sn-Beta-HF. Isomerization of glucose in flow over fresh (black) and recalcined (red) Sn-Beta-HF. Conditions: $T = 100\,^{\circ}C$, WHSV = $0.7\,h^{-1}$.

Table 2
Physicochemical properties of the fresh, spent and reused catalyst after glucose isomerization at 100 °C for 50 h.

Material	WHSV (h^{-1})	Sn-content (wt%)	S_{BET} (m^2/g)	V_{micro} (cm^3/g)	V_{meso} (cm^3/g)
Fresh	–	1.79 ± 0.01	530	0.21	0.05
Spent	0.7	n/a	427	0.15	0.11
Spent-calcined	–	1.76 ± 0.01	480	0.19	0.07
Spent-reused	0.7	n/a	481	0.14	0.16
Spent-reused-calcined	–	1.79 ± 0.03	552	0.20	0.14

hydrothermal stability of the material.

Pérez-Ramírez and co-workers reported that carrying out dihydroxyacetone (DHA) isomerization in methanol to methyl lactate led to a more stable operation than the reaction in water with lactic acid as the dominant product [34]. Previously, we reported that glucose isomerization proceeds at higher reaction rate in an ethanol/water (v/v = 9/1) mixture than in water, which is due to a decreased competition of ethanol with the active sites [52]. We expect that the decreased proton activity in such solvents results in a lower rate of formation of oligomeric products. Therefore, we carried out the reaction at 90 °C and at a WHSV of $1.5\,h^{-1}$ in ethanol/water (v/v = 9/1). Fig. 10a compares the catalytic performance of Sn-Beta-HF-large in water and water/ethanol solvents. Compared to operation in water, during which more than half of the activity was lost in the first 24 h, carrying out the reaction in the ethanol/water mixture resulted in nearly stable catalytic performance at a glucose conversion level around ~40% and a fructose yield of 20%. Small amounts of mannose and talose were observed. We verified that operation in the ethanol/water mixture did not significantly affect the textural properties. In particular, the micropore and mesopore volumes of the spent catalyst were nearly similar to those of the fresh catalyst (Table 3). Furthermore, no damage to the catalyst was observed in TEM (Fig. S6c).

In batch experiments, the pH of the reaction mixture decreased to

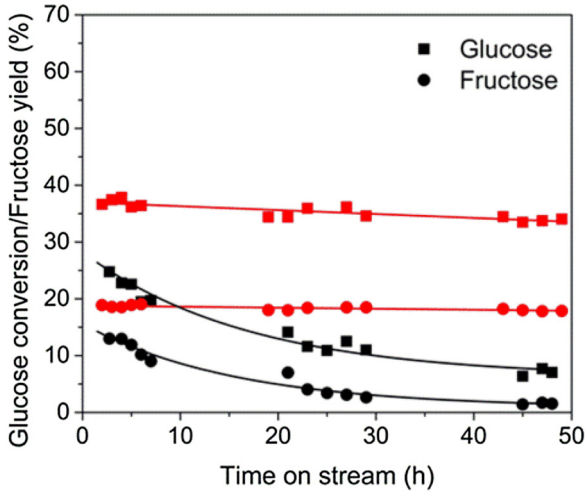

Fig. 10. Glucose isomerization in a flow reactor at a WHSV of 1.5 h^{-1} at 90 °C in water (black line) and ethanol/water (v/v/ = 9:1) (red line).

Table 3
Physicochemical properties of the fresh and spent Sn-Beta-HF before and after glucose isomerization at 90 °C for 50 h in water and ethanol/water (v/v = 9/1).

Solvent	WHSV (h^{-1})	Sn-content (wt%)	S_{BET} (m^2/g)	V_{micro} (cm^3/g)	V_{meso} (cm^3/g)
–	–	1.79 ± 0.01	530	0.21	0.05
Water	1.5	1.76 ± 0.01	398	0.15	0.08
EtOH/water 9:1	1.5	1.83 ± 0.04	447	0.19	0.05

Table 4
Physicochemical properties of Sn-Beta-HF after exposure in flow to water, 0.2 wt% lactic acid in water and 250 mM DHA in water at 100 °C.

Feed	M_{cat} (mg)	Flow (mL/min)	Sn-content (wt%)	S_{BET} (m^2/g)	V_{micro} (cm^3/g)	V_{meso} (cm^3/g)
–	–	–	1.79 ± 0.01	530	0.21	0.05
Water	125	0.25	1.95 ± 0.01	464	0.15	0.21
0.2 % LA	125	0.25	1.76 ± 0.01	488	0.16	0.16
250 mM DHA[a]	250	0.28	1.95 ± 0.01	423	0.14	0.26

[a] WHSV = 3.0.

3–4 during glucose isomerization. This pH decrease was also noted in the effluent during the first period of the continuous flow reaction experiments. The presence of small amounts of lactic acid was previously determined by in situ NMR spectroscopy as one of the by-products formed inside the zeolite pores during sugar conversion at 100 °C [52]. Lactic acid is formed via a sequential retro-aldolization-isomerization reaction from fructose. Accordingly, we suspect that organic acids such as lactic acid cause the pH decrease and damage the zeolite. We therefore investigated the effect of hydrothermal treatment of Sn-Beta catalysts in the presence and absence of lactic acid as a model compound for acid formation during glucose isomerization.

In another experiment, DHA was fed in order to elucidate the effect of the presence of substantial amounts of lactic acid as by-product in sugar conversion reactions (Table 4). The corresponding time-on-stream plot is shown in Fig. S5. Further experiments included demineralized water and 0.2 wt% aqueous lactic acid solution (pH ≈ 3) as blank measurements. We found that desilication took place both when 250 mM aqueous DHA and demineralized water were used as feed, which is corroborated by the increase in Sn-content of the catalysts. The kinetic data shown in Fig. S5 reveal that also here deactivation took place, going from 44% conversion to 20% conversion over 50 h of reaction. Furthermore, a significant increase of the mesopore volume was observed in the spent catalysts, from 0.05 cm3/g for the fresh catalyst to 0.21 and 0.26 cm3/g after exposure to demineralized water and 250 mM DHA, respectively at 100 °C. Under acidic, non-reactive conditions, a much smaller but still noticeable increase of the mesopore volume was observed (0.16 cm3/g). However, no loss of Sn was observed. Desilication has earlier been observed for a mesoporous organosilica used under hydrothermal conditions [53]. The use of a small amount of lactic acid did not lead to an increase in the Sn content, although the damage to the structure was still evident from the textural data. This may indicate that different mechanisms contribute to the damage of the zeolite framework. The formation of mesopores can also be derived from the TEM images (Fig. S6). The damage is most severe during DHA isomerization. Interestingly, in this case it was also seen that small particles were present on the surface of the damaged spent zeolite particles. We surmise that these are SnO_2 particles, caused by Sn removal from the framework and subsequent agglomeration into SnO_2. This effect was particularly evident during exposure to the acidic solvent (0.2 wt% LA, Fig. S6f), but was also visible in water (Fig. S6e). This shows that, although no Sn loss could be observed, under such conditions restructuring of the catalyst takes place, whereby Sn is removed from the framework.

4. Conclusions

The purpose of this work was to investigate the deactivation mechanism of Sn-Beta during sugar conversion reactions. Under stringent conditions of glucose retro-aldolization in methanol at 160 °C, oligomeric species are deposited in the zeolite micropores that rapidly deactivate the catalyst. The nature of these species and location was determined by a combination of UV–vis and IR spectroscopy and confocal fluorescence microscopy of the spent catalysts. While polyaromatic coke is predominant on H-beta, lower molecular-weight furanics, likely humin precursors, are the species that deactivate Sn-Beta. In the relatively large zeolite crystals used in this work as model systems, these species predominantly accumulate in the outer regions of the crystals. Deposition of such deposits was also observed during glucose isomerization in water at 100 °C. The use of Sn-Beta zeolite under these conditions for the isomerization of glucose and 1,3-dihydroxyacetone in a flow reactor revealed a very strong and continuous deactivation. In addition to deposition of oligomers, the zeolite framework is damaged and Sn is leached from the zeolite. As a result, mesopores are formed and SnO_2 is deposited during glucose conversion. The adverse influence of hydrothermal deactivation on the zeolite can be countered by employing a more hydrophobic ethanol/water mixture as the solvent. This procedure did not only lead to improved stability but also a higher activity in glucose isomerization.

Acknowledgements

This work was performed in the framework of the CatchBio programme and the Joint Scientific Thematic Research Programme funded by the The Netherlands Organization for Scientific Research (NWO) and the Chinese Ministry of Science and Technology. J.R.M. acknowledges the Dutch Science Foundation (NWO) for his personal VENI grant.

Appendix A. Supplementary data

Supplementary material related to this article can be found, in the online version, at doi:https://doi.org/10.1016/j.apcata.2018.07.023.

References

[1] R. Bermejo-Deval, R.S. Assary, E. Nikolla, M. Moliner, Y. Román-Leshkov, S.-J. Hwang, A. Palsdottir, D. Silverman, R.F. Lobo, L.A. Curtiss, M.E. Davis, Proc. Nat. Acad. Soc. U. S. A. 109 (2012) 9727–9732.

[2] H.J. Cho, P. Dornath, W. Fan, ACS Catal. 4 (2014) 2029–2037.
[3] Q. Guo, F. Fan, E.A. Pidko, W.N.P. van der Graaff, Z. Feng, C. Li, E.J.M. Hensen, ChemSusChem 6 (2013) 1352–1356.
[4] T. Ennaert, J. Van Aelst, J. Dijkmans, R. De Clercq, W. Schutyser, M. Dusselier, D. Verboekend, B.F. Sels, Chem. Soc. Rev. 45 (2016) 584–611.
[5] M. Moliner, Y. Román-Leshkov, M.E. Davis, Proc. Nat. Acad. Soc. U. S. A. 107 (2010) 6164–6168.
[6] E. Taarning, S. Saravanamurugan, M.S. Holm, J. Xiong, R.M. West, C.H. Christensen, ChemSusChem 2 (2009) 625–627.
[7] C.M. Lew, N. Rajabbeigi, M. Tsapatsis, Ind. Eng. Chem. Res. 51 (2012) 5364–5366.
[8] E. Nikolla, Y. Román-Leshkov, M. Moliner, M.E. Davis, ACS Catal. 1 (2011) 408–410.
[9] R. De Clercq, M. Dusselier, B.F. Sels, Green Chem. 19 (2017) 5012–5040.
[10] P. Ferrini, J. Dijkmans, R. De Clercq, S. Van de Vyver, M. Dusselier, P.A. Jacobs, B.F. Sels, Coord. Chem. Rev. 343 (2017) 220–255.
[11] S. Tolborg, I. Sádaba, C.M. Osmundsen, P. Fristrup, M.S. Holm, E. Taarning, ChemSusChem 8 (2015) 613–617.
[12] M.S. Holm, S. Saravanamurugan, E. Taarning, Science 328 (2010) 602–605.
[13] M. Orazov, M.E. Davis, Proc. Nat. Acad. Soc. U. S. A. 112 (2015) 11777–11782.
[14] Iv. Zandvoort, Y. Wang, C.B. Rasrendra, E.R.Hv. Eck, P.C.A. Bruijnincx, H.J. Heeres, B.M. Weckhuysen, ChemSusChem 6 (2013) 1745–1758.
[15] C.H.L. Tempelman, X. Zhu, K. Gudun, B. Mezari, B. Shen, E.J.M. Hensen, Fuel Proc. Technol. 139 (2015) 248–258.
[16] J. Goetze, F. Meirer, I. Yarulina, J. Gascon, F. Kapteijn, J. Ruiz-Martínez, B.M. Weckhuysen, ACS Catal. 7 (2017) 4033–4046.
[17] X. Zhu, N. Kosinov, J.P. Hofmann, B. Mezari, Q. Qian, R. Rohling, B.M. Weckhuysen, J. Ruiz-Martinez, E.J.M. Hensen, Chem. Commun. (Camb.) 52 (2016) 3227–3230.
[18] C.H. Bartholomew, Appl. Catal. A Gen. 212 (2001) 17–60.
[19] A.N. Parvulescu, D. Mores, E. Stavitski, C.M. Teodorescu, P.C.A. Bruijnincx, R.J.M.K. Gebbink, B.M. Weckhuysen, J. Am. Chem. Soc. 132 (2010) 10429–10439.
[20] R.M. Ravenelle, F. Schüβler, A. D'Amico, N. Danilina, J.A. van Bokhoven, J.A. Lercher, C.W. Jones, C. Sievers, J. Phys. Chem. C 114 (2010) 19582–19595.
[21] D. Padovan, C. Parsons, M. Simplicio Grasina, C. Hammond, Green Chem. 18 (2016) 5041–5049.
[22] X. Zhang, K. Wilson, A.F. Lee, Chem. Rev. 116 (2016) 12328–12368.
[23] H.Y. Luo, J.D. Lewis, Y. Román-Leshkov, Ann. Rev. Chem. Biomol. Eng. 7 (2016) 663–692.
[24] D.W. Gardner, J. Huo, T.C. Hoff, R.L. Johnson, B.H. Shanks, J.-P. Tessonnier, ACS Catal. 5 (2015) 4418–4422.
[25] P.A. Zapata, J. Faria, M.P. Ruiz, R.E. Jentoft, D.E. Resasco, J. Am. Chem. Soc. 134 (2012) 8570–8578.
[26] J.P. Lange, Angew. Chem. Int. Ed. 54 (2015) 13186–13197.
[27] C. Hammond, Green Chem. 19 (2017) 2711–2728.
[28] S. Prodinger, H. Shi, S. Eckstein, J.Z. Hu, M.V. Olarte, D.M. Camaioni, M.A. Derewinski, J.A. Lercher, Chem. Mater. 29 (2017) 7255–7262.
[29] A. Vjunov, M. Wang, N. Govind, T. Huthwelker, H. Shi, D. Mei, J.L. Fulton, J.A. Lercher, Chem. Mater. 29 (2017) 9030–9042.
[30] C. Sievers, Y. Noda, L. Qi, E.M. Albuquerque, R.M. Rioux, S.L. Scott, ACS Catal. 6 (2016) 8286–8307.
[31] I. Sadaba, M. Lopez Granados, A. Riisager, E. Taarning, Green Chem. 17 (2015) 4133–4145.
[32] I.W.C.E. Arends, R.A. Sheldon, Appl. Catal. A Gen. 212 (2001) 175–187.
[33] P.Y. Dapsens, C. Mondelli, J. Jagielski, R. Hauert, J. Perez-Ramirez, Catal. Sci. Technol. 4 (2014) 2302–2311.
[34] G.M. Lari, P.Y. Dapsens, D. Scholz, S. Mitchell, C. Mondelli, J. Perez-Ramirez, Green Chem. 18 (2016) 1249–1260.
[35] M.H.F. Kox, E. Stavitski, J.C. Groen, J. Pérez-Ramírez, F. Kapteijn, B.M. Weckhuysen, Chem. Eur. J. 14 (2008) 1718–1725.
[36] I.L.C. Buurmans, J. Ruiz-Martínez, W.V. Knowles, D. van der Beek, J.A. Bergwerff, E.T.C. Vogt, B.M. Weckhuysen, Nat. Chem. 3 (2011) 862.
[37] A. Corma, L.T. Nemeth, M. Renz, S. Valencia, Nature 412 (2001) 423.
[38] W.N.P. van der Graaff, G. Li, B. Mezari, E.A. Pidko, E.J.M. Hensen, ChemCatChem 7 (2015) 1152–1160.
[39] S. Mintova, V. Valtchev, T. Onfroy, C. Marichal, H. Knözinger, T. Bein, Microporous Mesoporous Mater. 90 (2006) 237–245.
[40] S. Tolborg, A. Katerinopoulou, D.D. Falcone, I. Sadaba, C.M. Osmundsen, R.J. Davis, E. Taarning, P. Fristrup, M.S. Holm, J. Mater. Chem. A Mater. Energy Sustain. 2 (2014) 20252–20262.
[41] M.S. Holm, Y.J. Pagan-Torres, S. Saravanamurugan, A. Riisager, J.A. Dumesic, E. Taarning, Green Chem. 14 (2012) 702–706.
[42] G.D. Manrique, F.M. Lajolo, Postharvest Biol. Technol. 25 (2002) 99–107.
[43] L.J. Webb, S. Rivillon, D.J. Michalak, Y.J. Chabal, N.S. Lewis, J. Phys. Chem. B 110 (2006) 7349–7356.
[44] J.W. Park, S.J. Kim, M. Seo, S.Y. Kim, Y. Sugi, G. Seo, Appl. Catal. A Gen. 349 (2008) 76–85.
[45] G. Spoto, F. Geobaldo, S. Bordiga, C. Lamberti, D. Scarano, A. Zecchina, Top. Catal. 8 (1999) 279.
[46] I.V. Sumerskii, S.M. Krutov, M.Y. Zarubin, Russ. J. Appl. Chem. 83 (2010) 320–327.
[47] M. Sevilla, A.B. Fuertes, Chem. Eur. J. 15 (2009) 4195–4203.
[48] G. Mirth, J.A. Lercher, M.W. Anderson, J. Klinowski, J. Chem. Soc., Faraday Trans. 86 (1990) 3039–3044.
[49] E.C. Nordvang, E. Borodina, J. Ruiz-Martínez, R. Fehrmann, B.M. Weckhuysen, Chem. Eur. J. 21 (2015) 17324–17335.
[50] M.K. Pyo, J.L. Jin, Y.K. Koo, H.S. Yun-Choi, Arch. Pharm. Res. 27 (2004) 381.
[51] K.A. Martin, R.F. Zabransky, Appl. Spectrosc. 45 (1991) 68–72.
[52] W.N.P. van der Graaff, C.H.L. Tempelman, G. Li, B. Mezari, N. Kosinov, E.A. Pidko, E.J.M. Hensen, ChemSusChem 9 (2016) 3145–3149.
[53] W.N.P. van der Graaff, K.G. Olvera, E.A. Pidko, E.J.M. Hensen, J. Molec. Catal. A: Chem. 388–389 (2014) 81–89.
[54] D. Padovan, S. Tolborg, L. Botti, E. Taarning, I. Sádaba, Ceri Hammond, React. Chem. Eng. 3 (2018) 155–163.
[55] M. Casagrande, L. Storaro, M. Lenarda, J. Gersich, L. Stievano, F.E. Wagner, T. Montanari, J. Mater. Chem. 14 (2004) 1010–1016.
[56] D. Padovan, L. Botti, C. Hammond, ACS Catal. 8 (2018) 7131–7140 8.